Impacts of Large-Scale NGSO Satellites: RFI and A New Paradigm for Satellite Communications and Radio Astronomy Systems

Yucheng Dai, *Student Member, IEEE*, Dong Han, *Student Member, IEEE*, and Hlaing Minn, *Fellow, IEEE*

***Abstract*— Large-scale non-geostationary orbit (NGSO) satellite communication systems (SCSs) are gaining interest from industries because of their ubiquitous wireless access and backhaul capabilities. However, the NGSO SCSs' global downlink transmission can cause radio frequency interference (RFI) to the radio astronomy system (RAS) on earth. Thus, this paper first investigates RFI impacts of a large-scale NGSO SCS. Our RFI analyses show that a large-scale low earth orbit (LEO) SCS completely disrupts RAS's continuum observation within or adjacent to the SCS downlink bands, which limits coexistence and growths of both SCS and RAS. To overcome such limitation, we propose a new paradigm where SCS and RAS are integrated into the NGSO satellite system, thus effectively creating large-scale telescopes in orbit. This integrated system not only avoids SCS's RFI to RAS but also offers more spectrum access opportunities to both SCS and RAS. In addition, this paper addresses two related problems of the new paradigm, namely, the spectrum resource allocation problem and the RAS data transport problem. Our performance evaluation illustrates the advantages of the proposed paradigm in terms of accessible spectrum bands, RAS observation performance, and SCS maximum mean supportable data rate as well as enabling coexistence and growths of both types of services.**

***Index Terms*— RFI mitigation, NGSO satellites, radio astronomy, integrated system.**

I. Introduction

NON-GEOSTATIONARY orbit (NGSO) satellite communication systems (SCSs), namely low earth orbit (LEO) and medium earth orbit (MEO) systems, have been investigated for decades. However, the unsuccessful commercial applications of the former NGSO systems launched decades ago have reduced further effort to promote such systems for years [2]. Recently, due to the increasing demand for ubiquitous high-speed and low-latency Internet connections as well as the rapid development of low-cost commercial spacecraft launching [3], [4], the space industry is planning to launch thousands of NGSO satellites. For instance, companies such as OneWeb and SpaceX are proposing to launch thousands of LEO and MEO satellites [5], [6]. These future NGSO satellites will form a tremendous space backhaul network via inter-satellite links (ISLs) [7] as well as a ubiquitous global wireless access network.

Radio astronomy provides a description of the universe and enables testing of laws of fundamental physics, e.g., General Theory of Relativity [8]. It is expanding from a phenomenological science to astro-physics and astro-chemistry for which the observations are intrinsically sensitivity-limited and interference-free environments are needed. Similarly, advances in radio astronomy require more and more radio astronomical observations (RAO) outside the frequency bands allocated to radio astronomy system (RAS) [9].

However, the prospects of large-scale NGSO SCSs cast a distressing RFI situation to RAS. The ground-based RAS uses highly sensitive receivers to observe very weak signals from cosmic sources within a wide frequency range. Out-of-band spectrum sidelobes from satellite transmitters, which are negligible to other communication systems, could substantially disrupt RAO. Furthermore, due to inherent nonlinearity of some transmitter components as well as device imperfection, unintended/unexpected RFI from satellites to RAS can occur. Although some efforts have been made to mitigate the RFI from active wireless services (including satellite communication) to the ground RAS, e.g., setting up Radio Quiet Zones (RQZs) [10], [11], blanking and excision [12]–[18], beamforming and spatial filtering approach [19]–[27], auxiliary antenna based RFI removal [28]–[31] and time-division sharing [32]–[37], unfortunately, their applicability to the large-scale NGSO systems is very limited. As large-scale NGSO systems plan to cover most of the earth surface ubiquitously, radio observatories on earth cannot hide from NGSO satellites' potential RFI. As an example, we can recall the Iridium satellite system with 66 LEO satellites launched in 1998. Even though several attempts were made to avoid RFI to RAS, in practice RAO data were corrupted by Iridium's RFI as confirmed in the new measurements conducted in 2010 [38].

In facing potential strong RFI from the large-scale NGSO SCSs, space-based radio telescopes are attractive solutions as they may have higher orbit than the NGSO SCSs and therefore

Manuscript received September 4, 2018; revised January 25, 2019 and April 30, 2019; accepted June 18, 2019. This work is supported by the National Science Foundation under Grant No. 1907614. Part of the materials was presented at IEEE ICC 2018 [1]. The associate editor coordinating the review of this paper and approving it for publication was A. Nallanathan. *(Corresponding author: Hlaing Minn.)*

The authors are with the Department of Electrical and Computer Engineering, The University of Texas at Dallas, Richardson, TX 75080-3021 USA (e-mail: hlaing.minn@utdallas.edu; yucheng.dai@utdallas.edu; dong.han6@utdallas.edu).

Color versions of one or more of the figures in this paper are available online at http://ieeexplore.ieee.org.

Digital Object Identifier 10.1109/TCOMM.2019.2928537

receive less RFI than the ground telescopes. In addition, the space-based telescope like HALCA [39] or Spektr-R [40] can form a Very Long Baseline Interferometry (VLBI) with ground telescopes to increase RAO performance. However, due to the cost and other issues, the number of the space-based radio telescopes is very limited and the overall performance of the existing space based radio telescopes is not compatible with the ground telescopes.

Motivated by both the critical conflict between the next generation NGSO SCS and RAS and the higher performance demands of RAS, we propose a new paradigm which overcomes the issues of the existing paradigm and offers several additional advantages. The new paradigm changes NGSO SCS into an integrated NGSO satellite communication and radio astronomy system (SCRAS) where satellites provide both RAO and communication services. The direct benefits are that RAS gains more RAO opportunities and performance enhancements (in terms of sensitivity through combining as in [35] and [36] and resolution through VLBI) and SCS obtains higher throughput and new services or business opportunities. The proposed approach offers a new infrastructure and paradigm at the side of data acquisition from radio astronomical objects. It is in synergy with the recent development of virtual astronomy observatory (VAO) [41] which is at the data processing side, offering a large scale electronic integration of radio astronomy data and tools for radio astronomers.

This paper's major contributions are summarized below.

- We analyze the RFI at ground radio telescopes caused by a large-scale NGSO SCS and investigate the required guardband bandwidth to keep RFI below the acceptable continuum observation threshold based on the emission mask requirement of National Telecommunications and Information Administration (NTIA). Then, we evaluate time and location dependent RFI caused by the OneWeb LEO system. Next, we assess the maximum baseline distance for VLBI observation and the number of telescopes that can observe the same target below the RFI threshold where both metrics are time-varying.
- We evaluate performance of RFI mitigation approaches such as guardband insertion, transmission muting, and sample excision, in the presence of large-scale OneWeb LEO SCS. Their RFI suppression performances, limitations, and costs in terms of SCS service degradation and RAO sample loss are assessed.
- We introduce a new paradigm for NGSO SCS and RAS by means of an integrated NGSO SCS and RAS, which not only eliminates the RFI from the devices operating below the NGSO but also offers additional advantages for both NGSO SCS and RAS.
- We investigate RAO performance of the proposed paradigm in terms of the observable bands without RFI concern, the average number of telescopes that can simultaneously observe a target, the maximum baseline distance for various target directions, and the observation sensitivity.
- As the bands originally allocated to RAS can be released to the integrated SCS and RAS system, we also address spectrum access and resource allocation in these bands and conduct corresponding data rate analysis for both SCS data and RAO data.
- Since the proposed paradigm conducts RAO in space, we develop a design of RAO data transport from satellites to ground stations, and evaluate its performance.

TABLE I
NOTATIONS USED IN THIS PAPER

Notation	Description
$\mathrm{epfd}_{i,j,k}(t)$	Instantaneous RFI epfd from satellite j's kth beam to ground telescope i at time t
$\overline{\mathrm{epfd}}_i(T)$	Average RFI epfd received by telescope i during RAO integration time T
$G_{\mathrm{T},j,k}(t)$	Transmitting antenna gain of satellite j's kth beam to ground telescope i at time t in the RAO band
$G_{\mathrm{R},i,j}(t)$	Receiving antenna gain of telescope i to satellite j at time t in the RAO band
$P_{\mathrm{UE},j,k}$	Unwanted emission power of satellite j's kth beam in the RAO band
$d_{i,j}(t)$	Distance between satellite j and telescope i at time t
$\mathrm{psd}_{\mathrm{UE}}(f)$	Power spectrum density of the unwanted emission at frequency f
$p_{\mathrm{LEO,beam}}$	Transmitting power of a spot beam of a LEO satellite
$\Delta\phi_{j,j_{\mathrm{ref}}}(t)$	Propagation delay induced fractional phase difference between telescope j and j_{ref} at time t
$\tau_{j,j_{\mathrm{ref}}}(t)$	Propagation delay induced integer sample index difference between telescope j and j_{ref}
$\Delta f_j(t)$	Doppler shift of the RAO signal received by satellite j at time t
$P_{\mathrm{out},n}$	Outage probability of link n
$P_{\mathrm{out,req},n}$	Required/target outage probability of link n
λ_n	Mean of instantaneous traffic of link n
$\Lambda_{n,\max}$	Maximum value that λ_n can take without violating the outage requirement of link n
$\hat{C}_{\mathrm{SG},i}(P_{\mathrm{out,req,SG}})$	Minimum capacity in the SG link that needs to be assigned to SCS to meet the outage probability requirement $P_{\mathrm{out,req,SG}}$

The paper is organized as follows. Section II introduces the LEO satellite system and ground telescopes model, and analyzes the RFI level at ground telescopes caused by the LEO satellites' downlink. Section III proposes three alternative RFI reduction methods and points out that these methods cause service degradation to LEO SCS or data loss to RAS. Section IV presents a new paradigm for LEO SCS and RAS and discusses its observability improvement for RAS. Section V analyzes the data rate improvement for SCS in the proposed paradigm. Section VI addresses RAO data transport issue. Finally, Section VII concludes this paper. Key notations used in the paper are shown in Table I.

II. RFI Analysis for Ground Radio Telescopes Under a Large-Scale LEO SCS

A. Interference Calculation

As satellite communication is one of the major sources of RFI, the International Telecommunication Union Radiocommunication Sector (ITU-R) has already provided several recommendations about this issue. The ITU-R document [42]

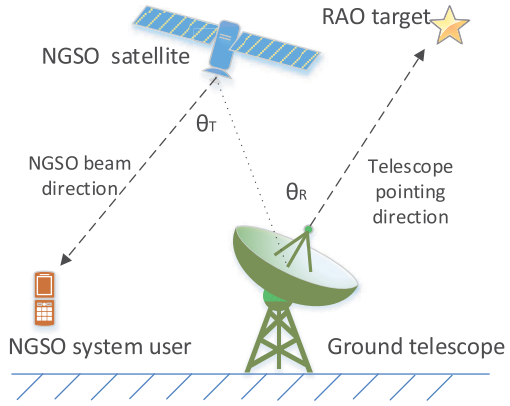

Fig. 1. An illustrative scenario for angles θ_{T} and θ_{R}.

offers a method to determine whether RFI is detrimental or not and some bands that should be protected from RFI. The ITU-R document [43] provides a method to calculate the RFI between NGSO satellites and radio telescopes based on the average equivalent power flux-density (epfd). The instantaneous epfd between telescope i and satellite j's kth beam at time t can be calculated with the following formula:

$$\mathrm{epfd}_{i,j,k}(t) = \frac{P_{\mathrm{UE},j,k} G_{\mathrm{T},j,k}(t) G_{\mathrm{R},i,j}(t)}{4\pi d_{i,j}^2(t)} \quad (1)$$

where $P_{\mathrm{UE},j,k}$ is the unwanted emission power of satellite j's kth beam in the RAO band, $G_{\mathrm{T},j,k}(t)$ is the transmitting antenna gain of the NGSO satellite j's kth beam towards the direction of telescope i at time t in the RAO band, $G_{\mathrm{R},i,j}(t)$ is the receiving antenna gain of telescope i towards the direction of satellite j at time t in the RAO band, and $d_{i,j}(t)$ is the distance between telescope i and satellite j at time t. Since $G_{\mathrm{T},j,k}(t)$ and $G_{\mathrm{R},i,j}(t)$ are determined by the relative positions of the satellite and the telescope, we have $G_{\mathrm{T},j,k}(t) = G_{\mathrm{T},j}(\theta_{\mathrm{T},i,j,k}(t))$ and $G_{\mathrm{R},i,j}(t) = G_{\mathrm{R},i}(\theta_{\mathrm{R},i,j}(t))$ where $\theta_{\mathrm{T},i,j,k}(t)$ is the angle between the boresight of the transmitting beam k and the direction from satellite j to telescope i at time t and $\theta_{\mathrm{R},i,j}(t)$ is the angle between the RAO direction and the direction from telescope i to satellite j at time t. Fig. 1 demonstrates a scenario of satellite and telescope we consider in the RFI calculation with θ_{T} and θ_{R}.

Then, for a certain RAO task conducted by telescope i, the average RFI at telescope i[1] during the integration time T_{int} can be represented as

$$\overline{\mathrm{epfd}}_i(T_{\mathrm{int}}) = \frac{1}{T_{\mathrm{int}}} \int_{t_0}^{t_0+T_{\mathrm{int}}} \sum_{j \in \mathbf{I}_{\mathrm{NGSO}}(t)} \sum_{k=1}^{N_{\mathrm{beam}}} \mathrm{epfd}_{i,j,k}(t)\ \mathrm{d}t \quad (2)$$

where t_0 is the beginning time of the RAO, $\mathbf{I}_{\mathrm{NGSO}}(t)$ is the index set of NGSO satellites that can be viewed from telescope i at time t and N_{beam} is the number of beams that each NGSO satellite uses for its downlink transmission. Due to the shape of the earth, not all LEO satellites are visible to a certain telescope. It is commonly assumed that only the visible satellites would cause RFI to RAO. Besides, in practice the integration time T_{int} can be 15 min, 1 hr, 2 hrs, 5 hrs, 10 hrs or other duration depending on the visibility of the RAO target and the required level of signal to noise ratio. Thus, we need to adjust the detrimental RFI threshold with respect to the integration time of each RAO task.

[1]The accumulated RFI at the telescope is a more appropriate metric than the RFI generated by a satellite as it determines RAO performance.

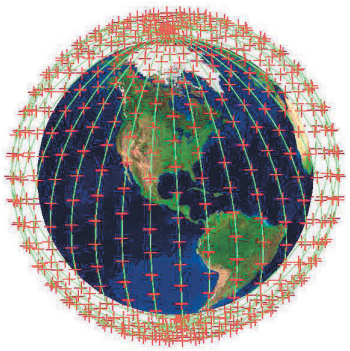

Fig. 2. OneWeb LEO satellite constellation (+ denotes a satellite).

B. Large-Scale LEO SCS Model: OneWeb

Although many companies propose their individual plans to build sky networks via a large number of LEO and MEO satellites, only a few of them (including OneWeb) have so far obtained the permission from Federal Communication Commission (FCC). In this paper, we use the constellation of OneWeb as our reference LEO satellites model. As mentioned in [44], there will be in total 720 LEO satellites running on circular orbits at 1200 km altitude. The satellites operate on 18 different orbital planes with 10 degree longitude spacing between two planes and each orbital plane has 40 LEO satellites. Fig. 2 shows a snap-shot of the OneWeb LEO satellite constellation. The red + symbol represents a LEO satellite and the green line connection between satellites indicates the path of the orbital plane. Each LEO satellite has 16 identical spot beams with fixed directions for communications with users. According to the description in [44], the spot beams should be highly elliptical to provide enough geographic coverage. However, as no detailed information is revealed in [44], we consider using a classical parabolic antenna model from [45] to simulate the downlink transmission of OneWeb LEO satellites. According to [44], the OneWeb user terminals will be equipped with mechanically steered parabolic reflectors and/or low-cost phased array designs with ability to track the on-the-move LEO satellites. The satellites will allow the users to switch from one spot beam to another, providing seamless network connection in continuous movement. Similar idea can be found in [46], [47]. In addition, as there are much fewer users on the ocean than users on land and the radio telescopes are located on land, we assume that the RFI effect of the beams pointing on the ocean is negligible. Table II shows other settings of the LEO satellites we consider in the paper, including the band assignment.

C. Ground Telescopes Model

In addition to the LEO satellites model, the ground radio astronomy telescopes model is another key factor in the

TABLE II
LEO SATELLITE SETTINGS

Parameter	Value	Parameter	Value
Orbital period	6565 sec	Bandwidth per beam	250 MHz
Tx power per beam $p_{\mathrm{LEO,beam}}$	7 Watt	Beamwidth (at 10.65 GHz)	10.1°
Boresight gain G_{T} (at 10.65 GHz)	24.4 dBi	Downlink band	10.7 – 12.7 GHz
Total downlink bandwidth per satellite	2 GHz	Frequency reuse factor	8

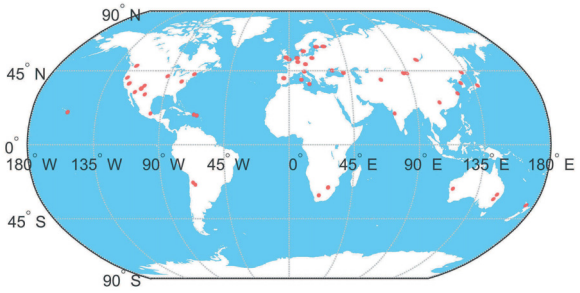

Fig. 3. Existing ground radio astronomy telescopes' locations.

performance evaluation. In this paper, we consider 58 existing observatories around the world as our reference ground radio astronomy telescopes model and assume all of them have the capability to observe the bands discussed in the paper. The red dots in Fig. 3 show the locations of these radio telescopes. We note that the distribution of ground radio astronomy telescopes is not even as more telescopes are located at the northern hemisphere (mostly in north America and west Europe). The unbalanced distribution of radio telescopes may cause some limitation for certain target directions. For simplicity, we consider the telescopes can observe the target with 10° minimum elevation angle to ensure that no detrimental ground interference leak into the telescopes. In addition, we assume that the ground telescopes have capability to observe both in daytime and nighttime as they can have large refrigeration and calibration systems to eliminate the effect of the solar illumination. Furthermore, as suggested by the ITU-R in [43], we consider the antenna model in [48] as the antenna model of the ground telescopes.

D. Guardband and Emission Mask Based RFI Analysis

From Eq. (1), we can see that the instantaneous RFI epfd level is related to the relative positions of the LEO satellites and the ground telescopes. To get more insight, let us consider a simplified model where one LEO satellite is at the zenith direction of a ground radio telescope and it has only one spot beam for downlink transmission. Suppose the radio telescope, as mentioned in [42], conducts a continuum observation in the 100 MHz bandwidth centered at 10.65 GHz and the LEO satellite uses a 250 MHz bandwidth of downlink near the RAO band. We first assume that the LEO satellite obeys the current unwanted emission requirements defined by FCC and NTIA [49], [50] and we will find the required guardband bandwidth between the RAO band and the satellite downlink band which satisfies the RFI threshold in Table 1 in [42]. The emission mask defines the maximum allowable emission power of the transmitter at frequency f. In this paper, we use an emission mask from NTIA [49], which limits the power spectrum density (psd) of the emission of inband signal at f based on the frequency offset $f_{\mathrm{off}} = |f_c - f|$, where f_c is the central frequency of the assigned band. Then, for any f out of the assigned band, the psd of the unwanted emission $\mathrm{psd}_{\mathrm{UE}}(f)$ should satisfy

$$\mathrm{psd}_{\mathrm{UE}}(f) \leq \mathrm{psd}_{\max} \cdot 10^{\frac{S_{\mathrm{EM}}(f_{\mathrm{off}})}{10}} \quad (3)$$

where $f_{\mathrm{off}} \geq \frac{B_{\mathrm{A}}}{2}$, B_{A} is the bandwidth of the assigned band,

$$S_{\mathrm{EM}}(f_{\mathrm{off}}) = \max\{-40 \cdot \log_{10}(\frac{2f_{\mathrm{off}}}{B_{\mathrm{A}}}) - 8, -60\}, \quad (4)$$

and $\mathrm{psd}_{\max}$ is the maximum psd of the satellite signals in the assigned band measured in a reference bandwidth [49]. Since $\mathrm{psd}_{\max}$ is related to the specific power distribution of the signals in the assigned band, without loss of generality, we consider $\mathrm{psd}_{\max} = \frac{p_{\mathrm{LEO,beam}}}{B_{\mathrm{A}}}$ in this paper where $p_{\mathrm{LEO,beam}}$ is the transmit power per a LEO satellite beam. In addition, we assume that the LEO SCS will generate the maximum allowable unwanted emission, and the unwanted emission power P_{UE} in the RAO band is

$$P_{\mathrm{UE}}(f_{\mathrm{RAO,L}}, f_{\mathrm{RAO,U}}) = \int_{f_{\mathrm{RAO,L}}}^{f_{\mathrm{RAO,U}}} \mathrm{psd}_{\max} \cdot 10^{\frac{S_{\mathrm{EM}}(f_{\mathrm{off}})}{10}} \mathrm{d}f \quad (5)$$

where $f_{\mathrm{RAO,L}}$ and $f_{\mathrm{RAO,U}}$ are the lower and upper edges of the RAO band, respectively. Eq. (5) also indicates that P_{UE} depends on the frequency separation between the SCS downlink band and the RAO band.

From Eq. (1), we can see that for a given θ_{T} and θ_{R} pair, we can find a corresponding P_{UE} that makes the RFI epfd meet the RFI requirement in Table 1 in [42]. One way to achieve this P_{UE} is to insert a guardband between the RAO band and the downlink band of the LEO satellite. Fig. 4 shows the relationship between (θ_{T}, θ_{R}) and the required guardband bandwidth. From the figure we can see that the required guardband bandwidth ranges from 150 MHz to 2375 MHz. From Eq. (3) and Eq. (4), we know that the minimum value of psd mask of the satellite downlink signals is $\mathrm{psd}_{\max} \cdot 10^{-6}$ when $f_{\mathrm{off}}/B_A \geq 1000\%$. Given $B_{\mathrm{A}} = 250$ MHz and $p_{\mathrm{LEO,beam}} =$ 7 Watt, inserting a guardband with bandwidth of 2375 MHz or larger yields a minimum P_{UE} of 2.8×10^{-6} Watt. Therefore, 2375 MHz can be viewed as the maximum effective guardband bandwidth as no lower unwanted emission power can be achieved via adopting a larger guardband bandwidth due to the flat emission mask floor. Consequently, there are some θ_{T} and θ_{R} pairs (e.g., $\theta_{\mathrm{T}} = \theta_{\mathrm{R}} = 0^\circ$) which make $G_{\mathrm{T}} \cdot G_{\mathrm{R}}$ too large that even the minimum P_{UE} cannot lower the RFI below the detrimental RFI threshold. However, since the LEO

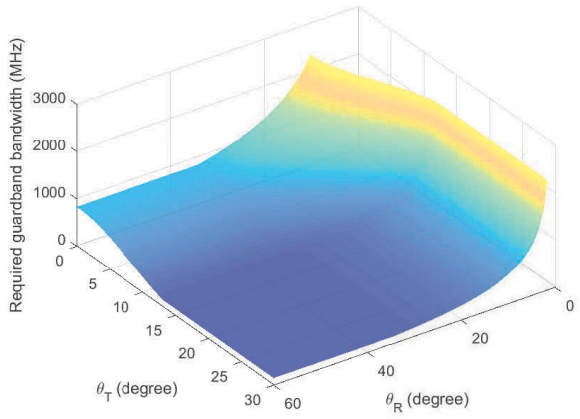

Fig. 4. The required guardband bandwidth versus $(\theta_{\mathrm{T}}, \theta_{\mathrm{R}})$.

satellites are moving fast, their relative positions with reference to a ground telescope will change from time to time and thus the instantaneous epfd will not always be such high. On the other hand, from Eq. (1) we can see that the lower bound of the required guardband bandwidth is related to the minimum value of G_{T} and G_{R} when the distance d is fixed. Fig. 4 indicates that the minimum required guardband bandwidth is 150 MHz for the considered $d = 1200$ km.

E. RFI Analysis Based on OneWeb LEO Constellation

In the previous section, we analyze the effects of θ_{T} and θ_{R} angle pairs on RFI assuming the distance between the LEO satellite and the radio telescope is fixed. However, since the LEO satellites are moving fast in the space (e.g., the OneWeb satellites have an angular velocity of 3.03°/min), we evaluate the average of the instantaneous RFI epfd under this practical scenario [43]. In this section, we consider a model that the ground radio telescopes are tracking a specific target in the far field, which can be viewed as fixed in the solar coordinate. Due to the blockage of the earth and the minimum elevation angle requirement, not all radio telescopes can observe the target at the same time. In addition, owing to the self-rotation of the earth, the ground telescopes may have their own certain time window to observe the target during a day, which is determined by their locations on the earth and the target direction. The RFI at the ground telescopes in the simulation comes from the downlink of the LEO satellites, which is, as mentioned in the previous sections, a band centered at 11.7 GHz with 2 GHz bandwidth and the ground telescopes are observing in the band 10.6 – 10.7 GHz.

Fig. 5 shows the instantaneous RFI epfd at a ground radio telescope along the observation time with the target direction at latitude $0°$ and longitude $180°$ in the earth coordinate when the RAO starts. From the figure we can see that the instantaneous RFI, although varies from time to time, has a fundamental period of approximately 2.7 min, which is the time interval between two successive LEO satellites in the same orbit that would fly across the main direction of the radio telescope. In addition, the envelope of the RFI would rise and fall as

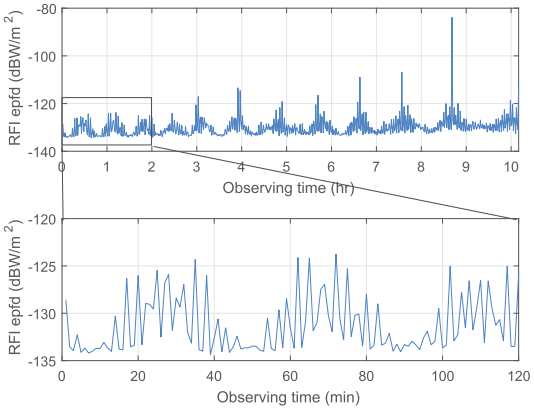

Fig. 5. Instantaneous RFI epfd at a ground telescope during 24 hours in the presence of LEO satellites.

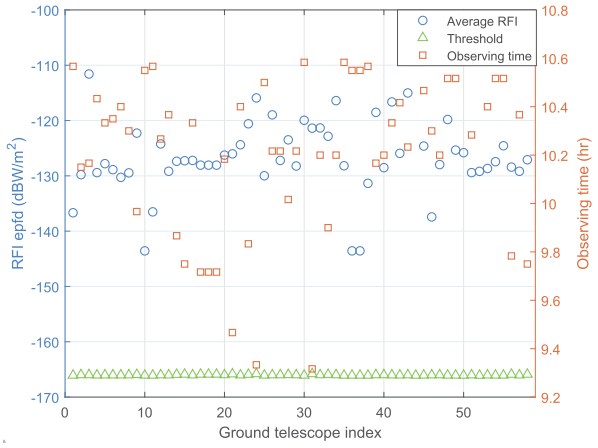

Fig. 6. Average RFI epfd levels at different ground telescopes during 24 hours in the presence of LEO satellites.

the RAO direction traverses the LEO orbital planes due to the earth's self-rotation.

Fig. 6 shows the average RFI levels of different ground radio telescopes with their corresponding RFI thresholds, which are determined by their respective observation time durations. It can be concluded from the figure that none of the ground telescopes are able to observe that certain target since the corresponding RFI are above the thresholds. In other words, the ground telescopes permanently lose the chance to observe this target in the presence of LEO satellites. For different ground telescopes, the average RFI epfd ranges from -144 to -110 $\mathrm{dBW/m^2}$, which has about 35 dB difference. Multiple factors may contribute to this difference, among which the dominant one is that the spot beams on ocean use much less transmitting power and thus cause negligible RFI to the ground telescopes. Consequently, the ground telescopes near or surrounded by the sea receive less RFI than the ones located inland.

In addition to the RFI at the telescopes when observing a certain target, we also numerically evaluate the RFI at certain telescopes with different azimuth and elevation angles of their own locations to show that the RFI from the LEO satellites affect almost all directions. Here we pick telescope 3 and 36 as

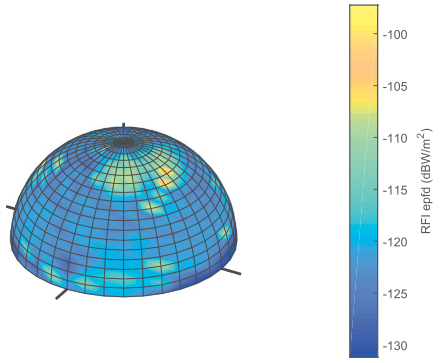

Fig. 7. Average RFI level at different azimuth and elevation angles of telescope 3 during 24 hours in the presence of LEO satellites.

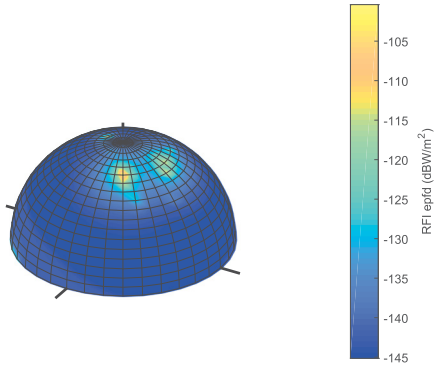

Fig. 8. Average RFI level at different azimuth and elevation angles of telescope 36 during 24 hours in the presence of LEO satellites.

our examples. Since telescope 3 is at North Liberty in Iowa and surrounded by land while telescope 36 is on the Big Island of Hawaii in the Pacific Ocean, the two are good representatives of the telescopes which face high level and low level of the RFI from the LEO satellites, respectively. Fig. 7 and Fig. 8 show the average RFI of the two telescopes during 24 hours. As we can see from the figures, the RFI peaks are usually located at directions with high elevation angles (e.g., $> 60^\circ$). Generally speaking, telescope 3 receives stronger RFI than telescope 36 in most directions. Both telescopes have average RFI epfd larger than $-160\ \mathrm{dBW/m^2}$, which is the ITU-R recommended RFI threshold for the observed band we consider with the 2000 seconds (sec) observation time.

The aforementioned analyses are based on continuum observation's requirements. Let us consider another possible situation where the ground telescopes can form a network and conduct VLBI observation. Since the VLBI observation has greater immunity to RFI, the threshold of VLBI observation is much looser than that for continuum observation. For the specific RAO band we consider in the previous sections, the threshold of VLBI observation ($-113\ \mathrm{dBW/m^2}$) is 47 dB higher than the threshold of continuum observation assuming 2000 sec observation time [42]. Besides the RFI, another key metric that affects the quality of the VLBI observation is the maximum baseline distance, which is defined as the maximum distance of any two radio telescopes that are observing a certain target at the same time.

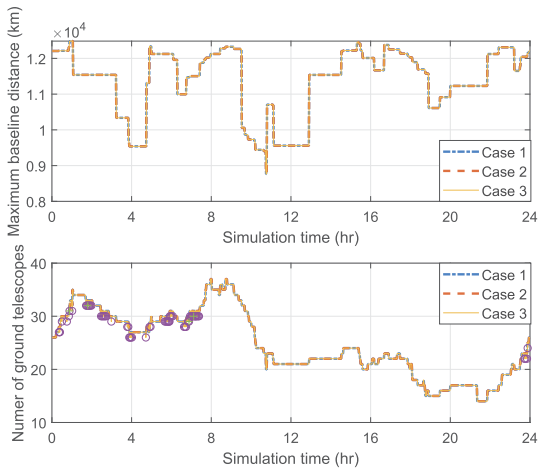

Fig. 9. Ground telescopes VLBI observation performance with and without LEO satellites.

To evaluate the performance of VLBI observation of the ground telescopes and the effect of the RFI, we plot the maximum baseline and the number of telescopes versus the observation time for the cases with and without RFI from the LEO satellites in Fig. 9. Here we consider three different cases, which are 1) the ground telescopes are completely RFI free in the RAO band (100 MHz centered at 10.65 GHz), 2) the ground telescopes have RFI from the LEO satellite downlink band (10.7 – 12.7 GHz) which is adjacent to the RAO band, and 3) the ground telescopes have RFI from the LEO satellite downlink band (10.6 – 12.7 GHz) which is in the RAO band. In this case, the downlink subband bandwidth of each spot beam is 262.5 MHz.

From Fig. 9, we can see that the maximum baseline distance of the ground telescope is not affected by the RFI even when the LEO satellites are using the RAO band as downlink. The number of telescopes that can observe the target is slightly affected by the RFI from the LEO satellites in the case 2 and 3, which are marked with green cross and purple circle respectively. But this degradation (0.011% and 0.178% sample loss in case 2 and 3) is insignificant in terms of the whole RAO process. The negligible degradation is owing to the higher detrimental RFI threshold for VLBI observation, which reflects immunity of VLBI observation against RFI. Another observation is that the distribution of the ground telescopes on earth surface is not even, and the number of ground telescopes and their maximum distance vary a lot during the RAO period. This variation may affect the performance of VLBI observation as during some of the time the number of telescopes that can observe is quite low (e.g., $<$15 telescopes) and the corresponding maximum baseline distance is relatively short (e.g., $<$9000 km).

III. Guardband, Transmission Muting and Sample Excision Based Solutions Under Large-Scale LEO SCS

From the previous section, we can see that the LEO satellites downlink transmission in adjacent bands of RAO will cause strong RFI in continuum observation. One potential solution is to temporally shut down the spot beams that may cause high

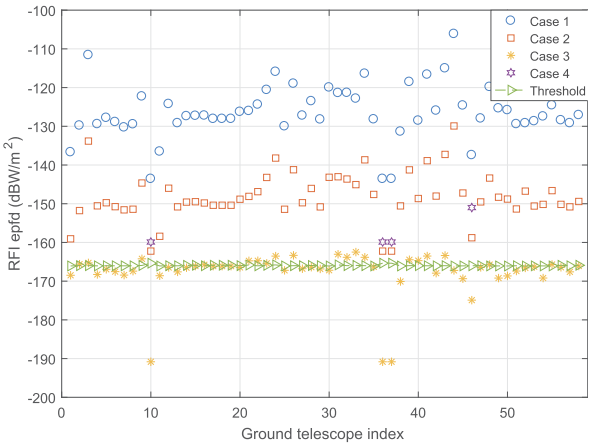

Fig. 10. Average RFI epfd levels at different ground radio telescopes for the 4 considered cases during 24 hours.

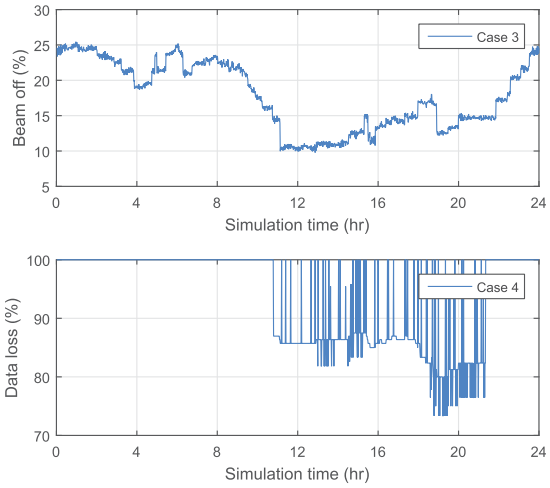

Fig. 11. Percentage of the beams that are turned off in case 3 and the instantaneous RAO sample loss rate in case 4 across time.

RFI epfd (e.g., larger than -180 dBW/m^2, which is 20 dB below the threshold in Table 1 in [42]). Here we assume that the LEO satellite system knows a priori the RAO plan of the ground radio telescopes (which is typically scheduled with much time in advance) and based on the locations and the observation direction of radio telescopes along with the orbital tracks of the LEO satellites, the system operator can determine the potential detrimental spot beams in advance. Another option is that instead of using all the assigned bandwidth for downlink transmission, the LEO satellite system will spare some bandwidth to be the guardband in between the RAO band and the satellite downlink band to reduce the RFI experienced at the telescopes. In addition, we can also let the ground telescopes drop the samples with high RFI to reduce to average RFI epfd levels. To compare the effects of the three methods, we consider the following 4 different cases:

1) No RFI reduction: No method is applied for RFI reduction. It is used as a reference.

2) Guardband approach: It inserts a 400 MHz additional guardband between the RAO band and the LEO SCS downlink band. Then, the subband of one beam is 200 MHz.

3) Transmission muting approach: It turns off the beams if they generate instantaneous RFI epfd at any of the ground telescopes higher than the threshold -180 dBW/m^2.

4) Sample excision approach: The ground telescopes drop the RAO samples with total instantaneous RFI epfd above the threshold -150 dBW/m^2.

Fig. 10 shows the average RFI epfd levels at different ground radio telescopes observing the same target as we use in the previous section for the four considered cases. From the figure we can see that, although the three aforementioned methods effectively reduce some RFI (approximately 18 dB – 25 dB for the guardband approach, 35 dB – 50 dB for the transmission muting approach and 10 dB – 15 dB for the sample excision method), there are still some of ground telescopes with average RFI epfd levels higher than the threshold even in case 3. Meanwhile, the transmission muting approach causes temporary communication service outage for some satellite users at some time, the guardband insertion approach leads to approximately 20% capacity loss in downlink, and the sample excision approach causes severe sample loss to the ground telescopes.

The percentage of the LEO satellites' beams which are shut down by the transmission muting approach during observation and the instantaneous RAO sample loss rate of the sample excision approach are shown in Fig. 11. From the figure we can see that at least 10% of spot beams are turned off during 24 hours and the corresponding users which are covered by these beams experience temporary connection loss. On the other hand, the ground telescopes may lose most of the RAO samples when the sample excision approach is applied during 24 hours and the overall RAO sample loss rate is 94.9%. In brief, these approaches are insufficient to handle the RFI issue of a large-scale NGSO SCS.

IV. A New Paradigm for NGSO SCS and RAS

A. An Integrated NGSO SCS and RAS

Since the three aforementioned methods cause unpleasant and inevitable service loss of the LEO SCS or sample loss of the RAO, a more efficient approach is needed to avoid RFI at telescopes for RAS and maintain communication service quality for SCS. For this, we propose a new paradigm in the form of an integrated NGSO satellite communication and radio astronomy system.

In the proposed paradigm, the communication satellites will be equipped with additional antennas and receivers to make RAO in addition to their main communication services. The zone for active communication services is towards the earth from the satellites while the one for RAO is from the satellites outwards the earth. Hence, the antennas for communication and RAO can be mounted at opposite sides of the satellite to each other. The satellites can use the RAO spectrum also in their active communication services as the spatial zones for the two services are non-interfering. Similarly, RAO can be made in the bands allocated for active wireless services. In other words, the communication satellites in the proposed paradigm now take the role of radio telescopes on earth for RAO in

exchange for their spectrum uses of the RAS spectrum for active communication systems. Satellites need to make RAO at a mutually agreed data rate and forward their RAO data through their earth-station gateways to RAS.

This innovation will benefit the NGSO SCS as follows:

- The bands in which NGSO systems can make sufficient RAO can be reused for active wireless services, thus offering more spectrum access opportunities for SCS.
- For the above bands, SCS will no longer need to implement RFI-avoiding mechanisms.
- SCS systems can obtain new services/business opportunities for additional RAO beyond their obligation.

The proposed paradigm offers RAS the following benefits:

- RAO from the satellites has signal strength gain due to the removal of atmospheric attenuation and weather impact (e.g., the space-based telescopes are free from atmospheric absorption which is especially severe in infrared, ultraviolet, 23 GHz, and 60 GHz bands and therefore are suitable to conduct photon detection and continuum/spectral line observation in these bands).
- The bands allocated for active wireless services which typically do not yield meaningful RAO at the ground telescopes (e.g., 10.7 – 12.7 GHz) can now be observed for RAS measurements.
- RFI from consumer electronic equipment and wireless systems, which are difficult to prevent from happening in practice, would not affect the RAO of the satellites.
- Due to large-scale NGSO systems, large-scale RAS telescope arrays infeasible with ground telescope systems can be realized.
- Large-scale NGSO satellites provide more RAO time than ground-based radio observatories.
- The proposed large-scale NGSO RAS can be combined with the existing ground RAS to yield a more capable RAS while avoiding conflicts with active wireless systems.

The following section will present more detailed RAO performance of the proposed paradigm.

B. Observability of LEO Versus Ground Telescopes

We assume that the LEO telescopes can observe within 60° from the zenith direction of the LEO satellites to avoid the RFI from earth surface and inter-satellite links. Furthermore, as mentioned in [51], the space based telescopes cannot make RAO (under cost constraint) if the sun illuminates the dish surface. Thus, we assume that the LEO telescope can observe when the sun is at least 90 degree from the zenith direction of the satellite. With this requirement, nearly half of the LEO telescopes cannot make RAO at each time instant due to the sun illumination. In addition, though we focus on the RAS bands near the satellites downlink in the previous sections, the LEO telescopes can observe not only in these bands but also in any other bands if they are equipped with corresponding receivers and if there are no RFI from the higher altitude SCSs. Specifically, since the LEO telescopes are above the atmosphere, they are very suitable for RAO in the bands with high atmospheric absorption (e.g., around 22 or 63 GHz) or with higher weather impact (e.g., $>$11 GHz) where the ground telescopes fail.

In Table III, we summarize five different types of bands and corresponding observability of ground and LEO telescopes with continuum and VLBI observation. The check-mark means the effect of RFI is negligible compared to the detrimental RFI threshold. We can see that except the bands used by SCSs with higher altitude than the proposed SCRAS, our proposed paradigm encounters less RFI than the ground telescopes and therefore gains more observability.

To evaluate the observability of the LEO telescopes versus the ground telescopes in VLBI observation, we focus on two key performance metrics which are the number of telescopes that can observe the same target simultaneously and the maximum baseline distance between those telescopes. To show the observability of the ground and LEO telescopes at different target directions, we first choose a reference direction in the earth coordinate, which is the opposite direction of the sun. As the time in simulation is relatively short with respect to the orbital period of the earth, we can assume the reference direction is fixed in the coordinate of the sun and represent other directions with relative latitude and longitude. For simplicity, we assume the date is equinox and the daytime and nighttime are of approximately equal duration all over the planet for all simulations except one example at winter solstice, which aims to show the performance variation of the LEO telescopes. In this section, we compare 5 potential VLBI observation cases, which are:

1) The LEO telescopes conduct VLBI observation at equinox.
2) The LEO telescopes conduct VLBI observation at winter solstice. Here we assume the same reference direction as in the previous case for comparison purpose.
3) The ground telescopes form a huge VLBI network and conduct VLBI observation at equinox. Its performance can be viewed as an upper bound of the ground telescopes.
4) The ground telescopes in Very Long Baseline Array (VLBA) conduct VLBI observation at equinox. The VLBA is a VLBI network with telescopes located in USA.
5) The ground telescopes in European VLBI Network (EVN) conduct VLBI observation at equinox. The EVN is a VLBI network with telescopes located in Europe and Asia.

Fig. 12 compares the average numbers of ground and LEO radio telescopes that can observe the same target simultaneously at several directions in cases 1, 2, 3, 4, and 5. The figure indicates the following.

- The plot of the number of the LEO telescopes forms a saddle-shaped distribution and the minimum number of LEO telescopes appears at the directions with relative longitudes $\pm 180^\circ$, (e.g., the direction of the sun) where the LEO telescopes cannot observe. The relative latitudes of the directions with the minimum number of the LEO telescopes are related to the subsolar point and therefore vary with different times of a year.
- Comparing the first two subfigures, we can see that when it is winter solstice, the astronomical polar night at the north polar region helps the LEO telescopes gain more observability in the north polar directions while at the

TABLE III
OBSERVABILITY OF THE LEO AND GROUND TELESCOPES

Band type/description	Ground telescope continuum observation	Ground telescope VLBI observation	LEO telescope continuum observation	LEO telescope VLBI observation
Bands within or adjacent to the downlink of the integrated SCRAS	Detrimental RFI blocks RAO in almost all directions	RFI with limited RAO data loss	✓	✓
Bands within or adjacent to the downlink of other large scale SCSs with **lower** altitude than the integrated SCRAS	Detrimental RFI blocks RAO in almost all directions[2]	RFI with limited RAO data loss[2]	✓	✓
Bands within or adjacent to the ground wireless communication, RADAR system or other active wireless systems	Without RQZ, RFI can cause potential RAO data loss	Without RQZ, RFI can cause potential RAO data loss	✓	✓
Bands within or adjacent to the downlink of other large scale SCSs with **higher** altitude than the integrated SCRAS	Detrimental RFI blocks RAO in almost all directions[2]	RFI with limited RAO data loss[2]	Detrimental RFI blocks RAO in almost all directions[2]	RFI with limited RAO data loss[2]
Bands with high atmospheric absorption or high weather impact	Opacity of the atmosphere blocks RAO	Opacity of the atmosphere blocks RAO	✓	✓

[2] Assuming no RFI reduction methods are applied.

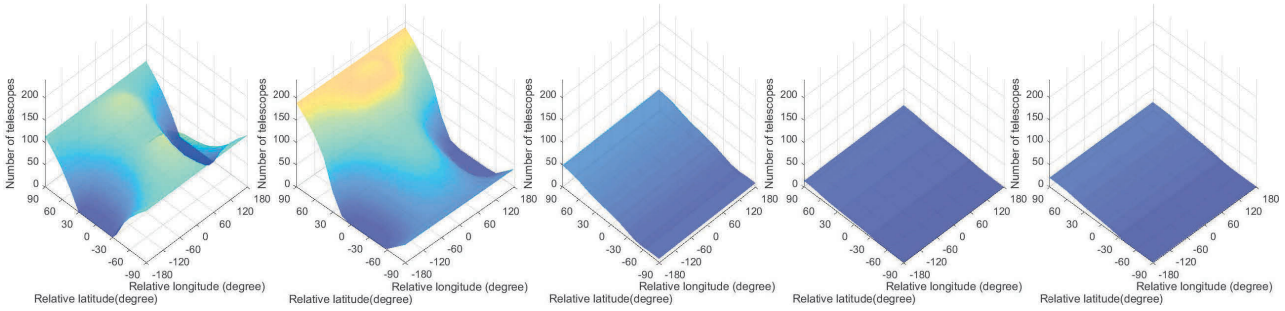

Fig. 12. Average number of telescopes that can simultaneously observe a target versus target directions (from left to right are case 1 to case 5).

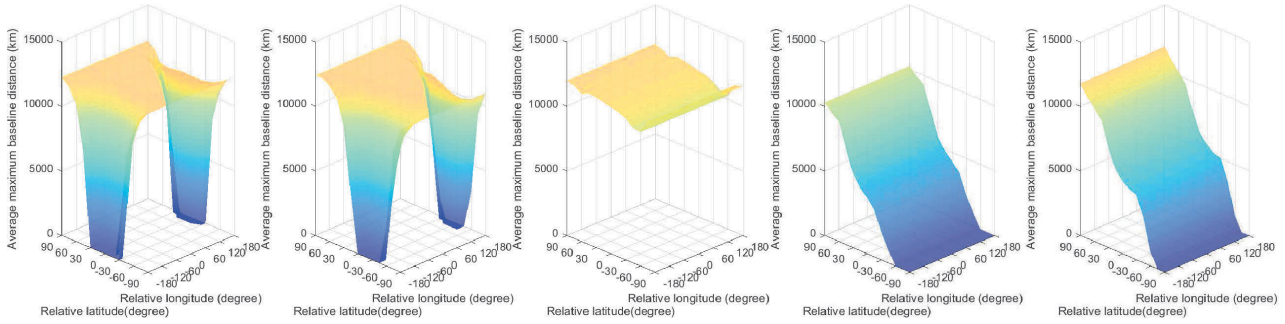

Fig. 13. Maximum baseline distance for different target directions (from left to right are case 1 to case 5).

same time the midnight sun at the south polar region decreases the number of the LEO telescopes that can conduct RAO. However, there are still at least 40 LEO telescopes that can observe the south polar directions simultaneously.

- Comparing subfigures 1, 3, 4, and 5, we can see that in most of the directions, there are more LEO telescopes than the ground telescopes that can observe. In addition, as most of the ground telescopes are located at the northern hemisphere, their observability is more in the north (positive relative latitude) than in the south (negative relative latitude).

Fig. 13 compares the maximum baseline distance of different observation directions averaged across time for the 5 cases. From the figure, we can observe the following.

- For the LEO and ground telescopes, the larger number of telescopes that can conduct observation simultaneously leads to the larger maximum baseline distance in the same direction. Nevertheless, comparing the maximum baseline distance of case 1 and 2 and the corresponding numbers in Fig. 12, we can see that the number of telescopes that can observe in the south polar direction ($-90°$ relative latitude) in case 1 is approximately 2 times of that in case 2, while the maximum baseline distance of the same direction in case 1 is only 10% larger than the one in case 2, which means the relationship between the number of satellites and the maximum baseline distance is non-linear.
- The first three subfigures indicate that the proposed LEO telescopes can achieve similar maximum baseline

distance as the upper bound of the ground telescope VLBI network in most directions at different times of the year except those that are affected by the sun.

- The last two subfigures reveal the poor performance of VLBA and EVN in terms of the maximum baseline distance in observing the south polar directions. The two existing VLBI networks lack of available telescopes in the south hemisphere of the earth and therefore lose some observability in those directions.

As we analyze in the previous sections, under the current ITU-R RFI threshold guideline the effect of the RFI from the LEO satellites to the ground telescopes is negligible for VLBI observation even if the satellites are using the RAO band as downlink. Under this circumstance, our proposed LEO telescopes can cooperate with current VLBI networks to improve the observation performance of both sides. For example, the LEO telescopes help the ground telescopes to improve their poor performance in the south hemisphere while the latter help the former cover the direction of the sun. Another notable aspect of the VLBI observation of the LEO telescopes is the timing synchronization. The LEO telescopes in the proposed paradigm will send the raw RAO data with time stamp to the ground gateways and further data synthesis and processing will be done at the ground data center. An accurate and reliable clock/time stamp can be established by using a fine-tuned internal clock (e.g., an atomic clock) or external clock (e.g., the GPS signals) or jointly using the two types of clocks. Similarly, the on-board clocks are synchronized before conducting RAO to ensure the accuracy of the time stamp. In addition, since the LEO telescopes are moving fast in the space, the Doppler effect of the astronomical signals needs to be considered. As the orbits of the LEO telescopes are known (as can be measured [52], [53]) in advance, the corresponding Doppler shift of the observed signals can be determined based on the telescopes' movements and the RAO target direction and therefore can be canceled in data processing. To explain further, denote the satellite location vector of satellite j at time t as $\mathbf{L}_j(t)$, the unit target direction vector as $\mathbf{D}(t)$ and the movement vector of satellite j as $\mathbf{V}_j(t)$. The inter-angle between the target direction and the zenith direction of the satellite i is given as $\theta_j(t) = \arccos(\frac{\mathbf{D}(t)\cdot\mathbf{L}_j(t)}{h})$ where h is the height of the satellite referred to the earth center. Assuming the maximum off-axis observation angle of the satellite-based telescope is θ_0, the index set of the telescopes that can observe the target at time t can be represented as $j \in \mathbf{I}_{\mathrm{T}}(t)$ such that $\theta_j(t) \leq \theta_0$. The movement (speed) of satellite j in the target direction is $\Delta V_j(t) = \mathbf{D}(t)\cdot\mathbf{V}_j(t)$. Given the sampling frequency f_s, the kth sampled signal on satellite j at time t can be represented as $s_j[k] \triangleq s_j(t = t_0 + k/f_s)$. Suppose the center frequency of the RAO band as f_{RAO}. Then the corresponding Doppler shift of satellite j's kth sample is $\Delta f_j[k] = \frac{\Delta V_j(t=t_0+k/f_s)}{c} f_{\mathrm{RAO}}$ where c is the speed of the light. The Doppler compensated baseband RAO signal can be represented as $s'_j[k] = s_j[k]\exp(-\sqrt{-1}\ 2\pi\Delta f_j[k]\frac{k}{f_s})$. After canceling the Doppler shift, the data processing center will synchronize the RAO data from different telescopes. The time delay for satellite j with reference to the center of earth is $\Delta\mathrm{T}_j(t) = -\frac{h}{c}\sin\theta_j(t)$ where the minus sign means the time when the signal of the target reaches the telescope is earlier than the time when it reaches the earth center (hypothetically). Then, the propagation delay induced fractional phase difference between telescope j and j_{ref} is $\Delta\phi_{j,j_{\mathrm{ref}}}(t) = 2\pi f_{\mathrm{RAO}}\cdot\mathrm{mod}(\Delta\mathrm{T}_{j_{\mathrm{ref}}}(t) - \Delta\mathrm{T}_j(t), \frac{1}{f_s})$ and the propagation delay induced integer RAO sample index difference between telescope j and j_{ref} is $\tau_{j,j_{\mathrm{ref}}}(t) = \lfloor(\Delta\mathrm{T}_j(t) - \Delta\mathrm{T}_{j_{\mathrm{ref}}}(t))/f_s\rfloor$ where $j, j_{\mathrm{ref}} \in \mathbf{I}_{\mathrm{T}}(t)$. For the given satellite network, $\{\Delta\phi_{j,j_{\mathrm{ref}}}(t),\ \tau_{j,j_{\mathrm{ref}}}(t)\}$ can be determined before conducting RAO. Then, the synchronization for the Doppler compensated baseband RAO signal $s'_j[k]$ of the satellite j can be performed at the ground RAO data processing center as $\{\exp(-\sqrt{-1}\ \Delta\phi_{j,j_{\mathrm{ref}}}(t))s'_j[k - \tau_{j,j_{\mathrm{ref}}}(t)]\}$ where $t = t_0 + k/f_s$.[3]

C. Sensitivity of LEO Versus Ground Telescopes

The sensitivity of the telescope reflects the lowest level of astronomical signals that can be detected by the telescope. To compare the RAO performance of the proposed system with the existing ground telescopes, we analyze the sensitivity performance of the proposed LEO telescopes and the ground telescopes. Based on [54], the sensitivity of a single dish telescope can be represented as

$$\Delta S_{\mathrm{single}} = \frac{2kT_{\mathrm{sys}}}{A_e\sqrt{T_{\mathrm{int}}B_{\mathrm{RAO}}}} \tag{6}$$

where B_{RAO} is the RAO band bandwidth, k is the Boltzmann constant, T_{sys} is the system noise temperature of the telescope, and A_e is the effective area of the telescope in the RAO band. A_e can be represented as $A_e = A_{\mathrm{phy}}\cdot\eta_{\mathrm{eff}}$ where A_{phy} is the physical aperture of the parabolic antenna and η_{eff} is the aperture efficiency of the antenna in the considered RAO band. For the telescope array with N_a identical telescopes (telescopes with identical hardware and levels of system noise), the sensitivity of the telescope array can be represented as

$$\Delta S_{\mathrm{array}} = \frac{2kT_{\mathrm{sys}}}{A_e\sqrt{N_a(N_a-1)T_{\mathrm{int}}B_{\mathrm{RAO}}}} \tag{7}$$

Specifically, as the ground telescopes may face the RFI from the NGSO satellites' downlink, the corresponding degradation should be considered. Therefore, we can refine Eq. (6) to incorporate the RFI from the NGSO satellites as

$$\Delta S'_{\mathrm{single}} = \frac{2kT_{\mathrm{sys}}(1+\kappa)}{A_e\sqrt{T_{\mathrm{int}}B_{\mathrm{RAO}}}} \tag{8}$$

where κ reflects the ratio between the RFI power and the system noise power. Here we consider a noise-like RFI which cannot be split from the desired astronomical signals. As mention in [42], the RFI should not introduce an error of 10% in measurement. In other words, the κ should be less than 10% to avoid corrupting the RAO data. However, from the analysis in Section II-E, we can see that the instantaneous RFI level generated by the OneWeb NGSO system will be 15 db – 50 dB higher than the detrimental RFI level, which

[3]The effects of the local oscillator induced phase offset on the VLBI measurements can also be identified and compensated, for example, by a typical calibration phase based on known target objects.

means that the κ can be up to 10000 (50dB higher than 10%). Under this condition, the RFI becomes the major source that severely limits the sensitivity of the ground telescopes.

To compare the sensitivity of the two types of telescopes, we choose ground telescopes with 25m (meter) (e.g., the VLBA telescope in Owens Valley, California) and 100m (e.g., the Green Bank telescope in Green Bank, West Virginia) dish sizes as the benchmarks to address the sensitivity advantages of the proposed LEO telescope array. The $T_{\rm sys}$ of the ground telescope in 10.6 – 10.7 GHz RAO band is considered to be 35 Kelvin (K) [42] as the ground telescope can use cryocooler to lower the system noise temperature. On the other hand, depending on the solar illumination as well as the cooling component(s) on the satellite (e.g., passive and/or active cooling component(s)), the system temperature of the LEO telescopes can be different. Therefore, we pick $\{35, 85, 135\}$ K [42] as the alternative system temperatures for the LEO telescopes. Note that the LEO telescope conduct RAO during nighttime and the temperature of the components can be as low as 70 K [55]. As the OneWeb satellites have limited size, the dish size of the LEO telescopes can not be too large. A conservative estimation of the dish size of the LEO telescopes is 3 meter. The aperture efficiency is assumed to be 0.15 [51] for both types of telescopes. Then, we can obtain the sensitivity of the proposed LEO telescope array as a function of the number of the telescopes in the array which are conducting the RAO to the same target simultaneously. The corresponding results are shown in Fig. 14. In addition, we show the sensitivity of the ground telescope with aforementioned dish sizes and levels of RFI from the LEO satellites in the figure. From the figure we can see that larger N_a can help the LEO telescopes to reduce the sensitivity level. Note that lower sensitivity level means the telescope can detect signal with lower power, which indicates better observation performance. Given enough number of LEO telescopes conducting RAO simultaneously (e.g., $N_a > 120$) and $T_{\rm sys} \leq 85$ K, the proposed LEO telescopes array have lower sensitivity level than the ground telescope has with 25m dish size even if no RFI is assumed at the ground telescope. However, due to the large difference of the effective area between the 100m ground telescope and the proposed LEO telescopes, the sensitivity level of the proposed LEO telescopes is higher than that of 100m ground telescope assuming no RFI at the telescope. Nevertheless, from the analysis in the previous section we can see that large-scale NGSO system will inevitably generate strong RFI to the ground telescopes and under such condition the proposed system can provide better sensitivity performance than the ground system as can be observed in Fig. 14.

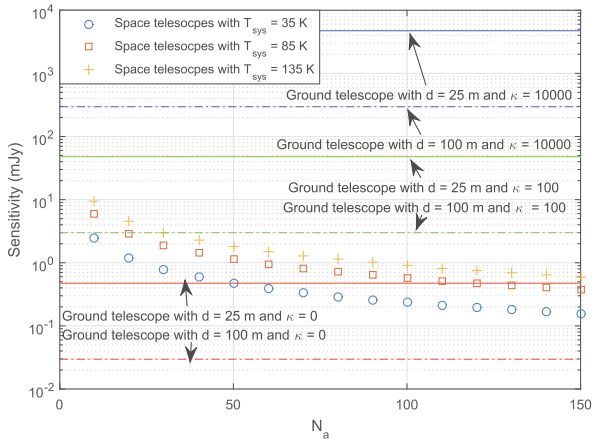

Fig. 14. Sensitivities of the ground and LEO telescopes.

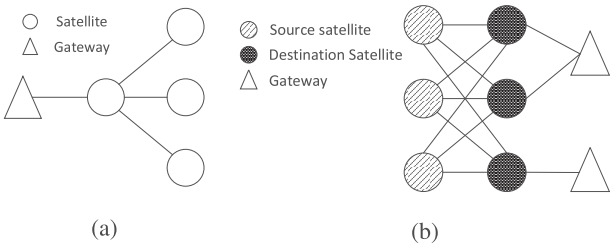

Fig. 15. System topological graphs. (a) Local graph for data rate analysis with $M = 4$. (b) Topological graph for RAO data transport with $L = 2$ and $N_{\rm s} = N_{\rm d} = 3$ (In practice, $N_{\rm s}$ could be greater than $N_{\rm d}$).

V. Data Rate Analysis Based on a Shared RAS Band in the Proposed Paradigm

A. Gateway-Satellite Model Based Data Rate Analysis

As mentioned in the previous sections, the LEO SCS may use the bands which are assigned to RAS while it provides RAS a network of LEO telescopes. To evaluate how much more data rate the new RAS bands can bring to the SCS, we consider a system model based on [44] which captures the essence of the data transmission in the SCS. Instead of considering all gateways and satellites in the SCS, we start analyzing the maximum supportable data rate of a certain gateway-satellite chain.

From [44], we can see that a gateway can directly connect to one specific LEO satellite via one antenna and other adjacent $M-1$ LEO satellites connect the gateway via this satellite, which means the directly connecting satellite serves as a relay for other satellites. An example of the topological graph is shown in Fig. 15(a) to illustrate the connectivities we consider in this section. Then, for the directly connecting satellite, there are 4 major links which are: satellite to gateway (SG) link, gateway to satellite (GS) link, satellite to user (SU) link and user to satellite (US) link. On the other hand, the remaining $M-1$ LEO satellites in the gateway-satellite chain only have their own SU and US links. We regard the traffics from multiple users within one satellite coverage as an aggregate traffic so that the SU broadcast link and the US multiple access link are simplified to point-to-point links. In addition, as the LEO telescopes need to send the observation data to the data processing center through the gateways, we also need to take this RAO data into account and evaluate the overall data rate of the aforementioned SCS model. We assume a fixed data rate $R_{\rm RAS}/M$ is reserved for RAO data downlink transmission for each satellite which results in an aggregate RAO data rate of $R_{\rm RAS}$ in the SG link. Besides, the traffic (in terms of packets per second) at the same satellite obeys a Poisson distribution

and each link has its own packet size. For a link n, the total capacity C_n can be represented as

$$C_n = \frac{\eta_n \mathcal{G}_n}{\beta_n} B_n, \quad n \in \mathcal{N} \tag{9}$$

where η_n, $\mathcal{G}_n$, β_n, and B_n are the spectrum efficiency, multiplexing gain, frequency reuse factor, and assigned bandwidth of link n and $\mathcal{N} = \{\mathrm{SU}, \mathrm{US}, \mathrm{SG}, \mathrm{GS}\}$. Then, we can define the outage probability of link n as

$$P_{\mathrm{out},n} = P(r_n > C_n), \quad n \in \mathcal{N} \tag{10}$$

where r_n is the instantaneous data rate, which can be represented as $r_n = \rho_n x_n$ with ρ_n and x_n being the packet size and instantaneous traffic (packets/sec) of link n. Then, the data rates of the 4 links are given by

$$\begin{aligned} r_{n,i} &= \rho_n x_i, \quad n \in \{\mathrm{SU}, \mathrm{US}\},\ i = 1, \ldots, M, \\ r_m &= \rho_m \sum_{i=1}^{M} x_i, \quad m \in \{\mathrm{SG}, \mathrm{GS}\}. \end{aligned} \tag{11}$$

Then, denoting the mean of x_n as λ_n, to meet the required outage probability $\mathbb{P}_{\mathrm{out},n}$, we can find a maximum mean supportable data rate (MMSDR) R_n as $R_n = \rho_n \Lambda_{n,\max},\ n \in \mathcal{N}$, where $\Lambda_{n,\max} = \max \lambda_n$ such that $P_{\mathrm{out},n} \leq P_{\mathrm{out,req},n}$. Specifically, for the SG link, as the SCS will provide RAO data transmission service to RAS side, a part of the data rate will be reserved for RAS data downlink transmission. Thus, we have $\Lambda_{\mathrm{SG},\max} = \max \lambda_{\mathrm{SG}}$ such that $P(r_{\mathrm{SG}} > C_{\mathrm{SG}} - R_{\mathrm{RAS}}) \leq P_{\mathrm{out,req,SG}}$. Assuming the average traffic ratio between the user downlink and uplink is $\zeta = \frac{\rho_{\mathrm{SU}}}{\rho_{\mathrm{US}}}$, we have $R_{\mathrm{SU}} = \zeta R_{\mathrm{US}}$ and $R_{\mathrm{GS}} = \zeta R_{\mathrm{SG}}$ where the second equation can be obtained from Eq. (11). Then, due to the cascaded nature of the links between users and gateways, we will have the maximum mean supportable data rate $\mathbb{T}_{\mathrm{GSU}}$ for the cascaded gateway-satellite-user (GSU) link, and $\mathbb{T}_{\mathrm{USG}}$ for the cascaded user-satellite-gateway (USG) link as $\mathbb{T}_{\mathrm{GSU}} = \min(R_{\mathrm{GS}}, M R_{\mathrm{SU}})$ and $\mathbb{T}_{\mathrm{USG}} = \min(R_{\mathrm{SG}}, M R_{\mathrm{US}})$. After that, we can have the overall MMSDR of the SCS as the sum of $\mathbb{T}_{\mathrm{GSU}}$ and $\mathbb{T}_{\mathrm{USG}}$.

From [44] we can see that the OneWeb LEO satellites use 4 different and discontinuous bands for the 4 different links. In this paper, we consider the SCS may exploit the shared RAS band in two potential modes: Time division Multiplexing (TDM) mode and Frequency Division Multiplexing (FDM) mode. In TDM mode, the SCS will let the four different links use different subframes at different times and each link can use the whole band during its own subframes. On the other hand, in FDM mode, each of the four links will use a sub-band of the RAS band and transmit information independently. Suppose link n uses α_n proportion of the shared RAS band (in TDM mode, the α_n can be viewed as the ratio of the number of subframes that are assigned to this link over the total number of subframes per frame), we can represent the new channel capacity of link n as

$$\tilde{C}_n = \frac{\eta_n \mathcal{G}_n}{\beta_n}(B_n + \alpha_n \Delta B), \quad n \in \mathcal{N} \tag{12}$$

where ΔB is the bandwidth of the shared RAS band. Note that in TDM mode, α_n can be adjusted according to the required RAS data rate due to the flexibility in subframe assignment while in FDM mode, α_n is fixed due to inflexibility/ infeasibility of filtering between different links. Then, the data rate maximization problem of the system can be represented as

$$\begin{aligned} &\max_{\{\alpha_n:\ n \in \mathcal{N}\}} \ \mathbb{T}_{\mathrm{GSU}} + \mathbb{T}_{\mathrm{USG}}, \\ &\text{s.t. } R_{\mathrm{SU}} = \zeta R_{\mathrm{US}}, \quad R_{\mathrm{GS}} = \zeta R_{\mathrm{SG}}, \ \sum_{n \in \mathcal{N}} \alpha_n + \alpha_0 = 1 \end{aligned} \tag{13}$$

where α_0 is the proportion of the shared RAS band that is assigned for guard band/period or other purposes and thus cannot be used for data transmission.

B. Communication System Maximum Mean Supportable Data Rate and RAO Data Rate Results

To evaluate the MMSDR of the integrated SCRAS, we consider 3 cases of band utilization in the proposed paradigm, which are i) the system uses the bands which are originally assigned to SCS only, ii) the system uses the original SCS bands and a shared RAS band in TDM mode, and iii) the system uses the original SCS bands and a shared RAS band in FDM mode. Note that when RAO data rate is 0, the performance of case 1 can be viewed as the performance of the original SCS. Table IV shows the parameters of the 4 links we use in the performance evaluation, which is originated from [44]. We choose the RAS band in 10.6 – 10.7 GHz as the example shared RAS band. In addition, we consider each link uses 20 MHz subband and the total guardband is 20 MHz in the FDM mode. For TDM mode we configure each frame with 100 subframes and each subframe has 1 ms duration. The guard period in TDM mode is 11 ms and equivalent to 11 subframes.

Fig. 16 shows the relationship between the RAO data rate per gateway and SCS MMSDR with different values of M and outage probability $\mathbb{P}_{\mathrm{out}}$ in the different band utilization cases. As we can see from the figure, both of the spectrum sharing modes (case 2 and 3) can afford more SCS data transmission than case 1 in general. In addition, due to the resource allocation flexibility, the TDM mode can achieve higher SCS MMSDR than the FDD mode. Comparing the SCS MMSDRs achieved by different modes, we can find out that SCS has approximately 1.1 Gbps more data rate in the TDM mode than in the original allocation when $M = 5$ and 0.33 Gbps more data rate when $M = 2$. In other words, if the integrated SCRAS maintains the same MMSDR supported by the original SCS (case 1 with 0 RAO data rate), it can support approximately 0.4 Gbps RAO data rate when $M = 5$ and 3.8 Gbps when $M = 2$ with the new band from RAS. Since the extra bandwidth of 0.1 GHz is relatively small compared with the SCS's original bandwidth of 6.9 GHz, the MMSDR improvement over the original SCS is limited. Nevertheless, several suitable RAS bands including 15.35 – 15.4 GHz, 22.21 – 22.5 GHz and, 23.6 – 24 GHz are around the LEO satellite downlink bands and therefore greater improvement can be achieved if the RAS side also shares these bands.

Fig. 16 also indicates how the bottleneck of the local system MMSDRs is affected by the aggregate RAO data rate and the

TABLE IV
PARAMETERS FOR THE LEO SCS LINKS

Link n	Assigned Bands (GHz)	Bandwidth (GHz)	Spectrum Efficiency η_n (bits/s/Hz)[4]	Multiplexing Gain $\mathcal{G}_n$	Frequency Reuse Factor β_n
User downlink (SU)	10.7 – 12.7	2.0	1	16	8
User uplink (US)	12.75 – 13.25, 14.0 – 14.5	1.0	1	16	8
Gateway downlink (SG)	17.8 – 18.6, 18.8 – 19.3, 19.7 – 20.2	1.8	4	2	1
Gateway uplink (GS)	27.5 – 29.1, 29.5 – 30.0	2.1	2	2	1

[4] Here we use a conservative setting. In practice, the spectrum efficiency depends on several system settings such as modulation type and SNR.

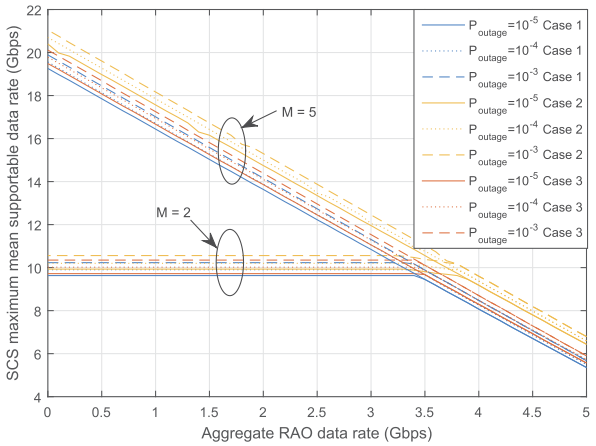

Fig. 16. Aggregate RAO data rate and SCS maximum mean supportable data rate of the proposed integrated system for 3 band utilization cases.

number of satellites supported by the gateway. For $M = 5$, the SG link is the bottleneck link of the local system. On the other hand, for $M = 2$, the bottleneck link changes from the US link to the SG link when the RAO data rate increases from below 3.5 Gbps to above 3.5 Gbps, which leads to slope changes of the corresponding curves. The different bottleneck links for $M = 2$ and 5 with the same RAO data rate are caused by the different SCS traffics on the SG link, which is related to the different values of M. Moreover, with the same bottleneck link, the two groups of curves ($M = 2$ and 5) overlap when $R_{\mathrm{RAS}} > 3.5$ Gbps. In this case, the RAO data occupies a large proportion of SG link capacity and the spectrum resource shared by RAS side is used only for increasing the capacity of the SG link.

VI. RAO DATA TRANSPORT DESIGN

A. Development of Data Transport

Data acquisition and transport are the two critical parts of an RAO mission. For an RAO, the suitable satellite positions on the orbital surface which meet the angle requirement between the target direction and the zenith direction of the LEO telescope can be represented by a dome centered at the target direction $\mathcal{C}$ with arc radius R_{ob}. Under this circumstance, the proposed SCRAS selects the L nearest gateways to the $\mathcal{C}$ for RAO data downlink transmission. In addition, we assume $N_{\mathrm{d},l}$ LEO satellites directly connect the lth selected gateway and the connections between the LEO satellites and the gateways are based on the nearest neighbor criterion. As mentioned in [44], a gateway can have 10 antennas (or more in some cases) and one antenna can establish a two-way link connection with one LEO satellite at a time. Therefore, for the performance evaluation in this section, we assume a gateway connects to at most the 10 nearest satellites above the minimum elevation angle and the satellite selects the nearest gateway to set up a two-way connection. Then, the total number of the gateway-connected satellites of the selected L gateways N_{d} can be represented as $N_{\mathrm{d}} = \sum_{l=1}^{L} N_{\mathrm{d},l}$ such that $N_{\mathrm{d},l} \leq 10$. A simple example of the connectivities among the involved satellites and gateways is shown in Fig. 15(b) to illustrate the considered problem. Then, with this model, we can analyze the relationship between the SCS traffic and the supportable RAS data rate and design the data transport strategy accordingly. Despite our analysis is based on a snap-shot of the whole RAO period, it can be extended to the whole RAO period by dividing the whole period into several fractional periods with fixed satellite-gateway connections.

Assume the SG link traffic from SCS side of satellite i can be represented as a Poisson random variable x_i (packets/second) with a mean value $\lambda_{\mathrm{SG},i}$ where $i = 1, \ldots, N_d$. To guarantee the SCS SG link data transmission within a required outage probability $P_{\mathrm{out,req,SG}}$ and accomplishing the RAO data transmission, the affordable RAO data rate of the ith satellite $R_{\mathrm{RAS},i}$ is

$$R_{\mathrm{RAS},i} = \max\{\tilde{C}_{\mathrm{SG},i} - \hat{C}_{\mathrm{SG},i}(P_{\mathrm{out,req,SG}}), 0\} \qquad (14)$$

where $\hat{C}_{\mathrm{SG},i}(P_{\mathrm{out,req,SG}})$ is the minimum capacity in the SG link that needs to be assigned to SCS to meet the outage probability requirement $P_{\mathrm{outage,req,SG}}$. Thus, the total supportable RAO data rate is $R_{\mathrm{RAS}} = \sum_{i=1}^{N_d} R_{\mathrm{RAS},i}$. Eq. (14) indicates that a larger RAO data rate can be accommodated with more gateways or at the cost of either higher SCS outage probability or smaller SCS average traffic using the same number of gateways.

After obtaining the total supportable RAO data rate of the selected gateways, another data transport problem is how to allocate the RAO data rate of the working LEO telescopes to the selected gateways. As the RAO data is transmitted from the working LEO telescopes to the N_{d} gateway-connected satellites via Inter-Satellite Links (ISLs), a primary concern of this procedure is the relaying cost of the data. Suppose the LEO telescope j in the RAO region generates RAO data with date rate s_j, and to make full use of the aggregate supportable RAO data rate and avoid congestion, we have

$\sum_{j=1}^{N_\mathrm{s}} s_j = R_\mathrm{RAS} = \sum_{i=1}^{N_\mathrm{d}} R_{\mathrm{RAS},i}$ where N_s is the number of the working LEO telescopes in the RAO region. Then, we can design the RAO data transport based on the N_s working LEO telescopes as the sources and the N_d gateway-connected satellites as the destinations.

Denoting the data flow (in terms of packets per second) from the jth source to the ith destination as $f_{j,i}$, we aim to minimize the total relaying cost of the RAO data by optimizing the allocation of the flows between the sources and the destinations. However, for a certain source and destination pair, there could be multiple paths depending on the connection topology of the satellite network and hence the corresponding relaying costs may vary. For the performance evaluation in this section, we define the relaying cost of a source and a destination as the number of ISL hops the data flow passed through. For simplicity, we consider no maximum rate constraint to the RAO data flow in ISLs and therefore the relaying cost from the jth source to the ith destination $c_{j,i}$ is determined by the path with the minimum number of ISL hops. Then, the minimum cost RAO data flow allocation problem can be formulated as

$$\begin{aligned} &\min_{\{0\le f_{j,i}\}} \sum_{j=1}^{N_\mathrm{s}}\sum_{i=1}^{N_\mathrm{d}} c_{j,i} f_{j,i}, \\ &\text{s.t.} \sum_{j=1}^{N_\mathrm{s}} f_{j,i} = R_{\mathrm{RAS},i}, \quad i = 1,\ldots,N_\mathrm{d}, \\ &\sum_{i=1}^{N_\mathrm{d}} f_{j,i} = s_j, \quad j = 1,\ldots,N_\mathrm{s}. \end{aligned} \tag{15}$$

This flow allocation problem can be recognized as a linear programming problem and therefore can be solved with some existing software such as MATLAB.

B. Data Transport Performance Results

In the simulation, we assume the RAO region is centered at 45°N 100°W with an observation radius $R_\mathrm{ob} = 3000$ km and 35 working LEO telescopes are in the region for the specific snap-shot we consider. We apply the same FDM settings in the previous section at all L gateways and assume the bandwidth of the RAS band assigned to the SG link is 100 MHz. In addition, the mean traffic $\lambda_{\mathrm{SG},i}$ of the ith satellite is generated by a Poisson distribution with the mean of 1200 packets/s. The RAO data rate of the working LEO telescopes is assumed to be same and fixed in the period we evaluate so that $s_j = R_\mathrm{RAS}/N_\mathrm{s},\ j = 1,\ldots,N_\mathrm{s}$. The simulation results are based on the average of 100 realizations of the random locations of the gateways (where the minimum distance between any two gateways is 1029 km) and of 100 realizations of the Poisson distributed traffics.

Fig. 17 shows the results of the aggregate supportable RAO data rate with different numbers of selected gateways under different outage probability requirements of SCS. For the same outage probability requirement, the aggregate supportable RAO data rate increases with the number of selected gateways, as more SG links are available. On the other hand, for the same amount of selected gateways, the larger SCS outage probability leads to large RAO data rate. The results

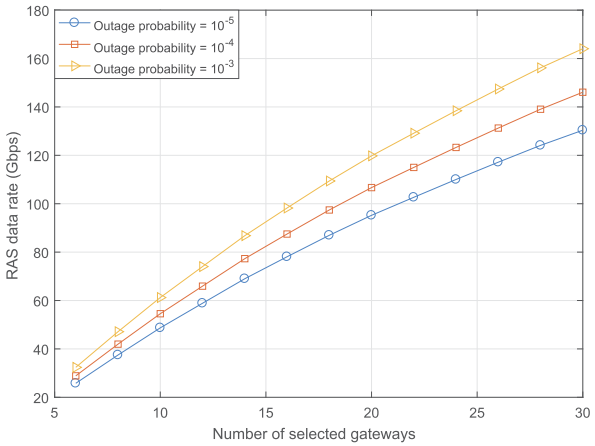

Fig. 17. RAO data rate versus the number of the selected gateways.

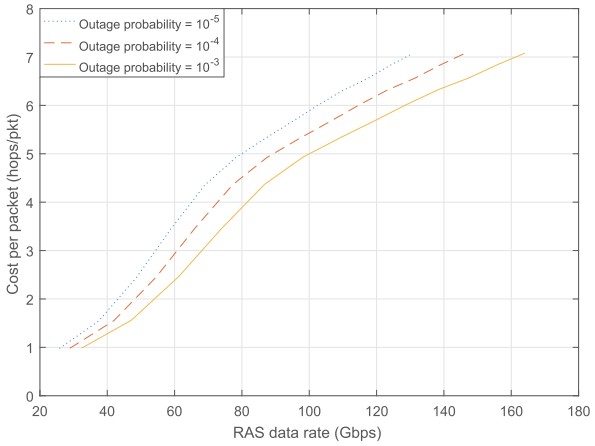

Fig. 18. RAO data packet relaying cost.

are consistent with the discussion of Eq. (14) in the previous subsection.

Fig. 18 demonstrates the relationship between the average relaying cost per packet and the aggregate RAO data rate under different outage probability requirements of SCS. From the figure we can see that the relaying cost increases with the RAO data rate. This can be explained by that the growing RAS data rate requires more gateways at farther locations from the RAO region center to be involved and consequently it increases the average relaying cost. In addition, the slope of the curves in the figure varies as the RAO data rate increases, which is caused by the non-uniformly distributed locations of the selected gateways. As the gateways can only be placed on land, the shape of the land will affect the distribution of the locations of selected gateways and therefore results in a non-constant slope of the curves. Furthermore, for the RAO data rate, the higher SCS outage probability results in lower relaying cost per packet, which is due to that more RAO data rate can be accommodated to the gateways with lower relaying cost.

VII. Conclusion

In this paper, we investigated the RFI effect of the emerging large-scale LEO satellite system (using OneWeb LEO satellite system as an example) on the ground radio telescopes. As the communication beams of the LEO satellites cover almost

our entire planet, the RFI to the ground radio telescopes is inevitable. Our evaluation shows that the potential RFI can be tens of dB above the acceptable interference threshold of the continuum observation, corrupting the radio astronomical observations in the LEO satellites' (adjacent) downlink bands. On the other hand, with inherent high immunity to the RFI, the VLBI observation can withstand the same level of RFI. To reduce the RFI from the emerging large-scale LEO satellites, we apply three existing methods namely transmission muting, guardband insertion, and samples excision method. Our numerical evaluation shows that although these methods successfully reduce the average RFI levels for some of the ground telescopes, they can cause significant capacity loss to the LEO satellite system or severe sample loss to the ground telescopes.

To address the large-scale LEO SCS's RFI issue and guarantee the performances of both the SCS and the RAS, we proposed an integrated NGSO satellite communication and radio astronomy system where the NGSO satellites are configured as an infrastructure for both SCS and RAS. With the proposed paradigm, the RAS can make continuum observation in the LEO satellite downlink bands as well as other bands if they are equipped the corresponding receivers in these bands. In addition, the LEO telescopes can achieve larger maximum baseline distance and larger number of simultaneous RAO in most directions in VLBI observation compared to the existing ground telescope VLBI networks. Moreover, as the proposed paradigm causes negligible data loss to the ground telescopes, the two types of telescopes can work together to further improve the performance of the VLBI observation. The sensitivity analysis also shows the advantages of the proposed space telescopes over the existing ground telescopes. With the shared RAS band, our new paradigm also increases the maximum mean supportable data rate of the SCS. Furthermore, we also developed a minimum cost RAO data transport design. Our results show that the data rates can be traded off between SCS and RAS, and a larger RAS data can be transported from space to ground at the cost of larger numbers of inter-satellite hops and gateways. Overall, the performance results collaborate that the proposed paradigm offers mutual benefits to both SCS and RAS and facilitates growth of both services.

REFERENCES

[1] H. Minn, D. Han, and Y. Dai, "A new paradigm for non-geostationary satellite communications and radio astronomy system," in *Proc. IEEE Int. Conf. Commun. (ICC)*, May 2018, pp. 1–7.

[2] J. Lim, R. Klein, and J. Thatcher, "Good technology, bad management: A case study of the satellite phone industry," *J. Inf. Technol. Manage.*, vol. 16, no. 2, pp. 48–55, 2005.

[3] O. Nizhnik, "A low-cost launch assistance system for orbital launch vehicles," *Int. J. Aerosp. Eng.*, vol. 2012, Apr. 2012, Art. no. 830536.

[4] J. Straub, "Cubesats: A low-cost, very high-return space technology," in *Proc. Reinventing Space Conf.*, 2012, pp. 1–6.

[5] W. Hanson, "A global Internet: The next four billion users," *New Space*, vol. 3, no. 3, pp. 204–207, Sep. 2015.

[6] V. L. Foreman, A. Siddiqi, and O. De Weck, "Large satellite constellation orbital debris impacts: Case studies of OneWeb and SpaceX proposals," in *Proc. AIAA SPACE Astronaut. Forum Expo.*, 2017, p. 5200.

[7] U. Siddique, H. Tabassum, E. Hossain, and D. I. Kim, "Wireless backhauling of 5G small cells: Challenges and solution approaches," *IEEE Wireless Commun.*, vol. 22, no. 5, pp. 22–31, Oct. 2015.

[8] M. Rosenberg, G. Bladon, P. Russo, and L. L. Christensen, "Astronomy in everyday life," *Commun. Astron. Public J.*, vol. 14, pp. 30–36, Jan. 2014.

[9] European Science Foundation, "Committee on Radio Astronomy Frequencies," *CRAF Handbook for Radio Astronomy*, 3rd ed. Groningen, The Netherlands: CRAF Secretariat, Netherlands Foundation for Research Astronomy, 2005.

[10] R. Umar, Z. Z. Abidin, Z. A. Ibrahim, Z. Rosli, and N. Noorazlan, "Selection of radio astronomical observation sites and its dependence on human generated RFI," *Res. Astron. Astrophys.*, vol. 14, no. 2, p. 241, Feb. 2014.

[11] W. Van Driel, "Radio quiet, please!–protecting radio astronomy from interference," *Proc. Int. Astronomical Union*, vol. 5, no. S260, pp. 457–464, Jan. 2009.

[12] R. Weber, C. Faye, F. Biraud, and J. Dansou, "Spectral detector for interference time blanking using quantized correlator," *Astron. Astrophys. Suppl. Ser.*, vol. 126, no. 1, pp. 161–167, Nov. 1997.

[13] A.-J. Boonstra, A. Leshem, A.-J. van der Veen, A. Kokkeler, and G. Schoonderbeek, "The effect of blanking of TDMA interference on radio-astronomical observations: Experimental results," in *Proc. IEEE Int. Conf. Acoust. Speech Signal Process. (ICASSP)*, vol. 6, Jun. 2000, pp. 3546–3549.

[14] W. Dong, B. D. Jeffs, and J. R. Fisher, "Radar interference blanking in radio astronomy using a Kalman tracker," *Radio Sci.*, vol. 40, no. 5, pp. 1–13, Oct. 2005.

[15] N. Niamsuwan, J. T. Johnson, and S. W. Ellingson, "Examination of a simple pulse-blanking technique for radio frequency interference mitigation," *Radio Sci.*, vol. 40, no. 5, pp. 1–11, Oct. 2005.

[16] Q. Zhang, Y. Zheng, S. G. Wilson, J. R. Fisher, and R. Bradley, "Excision of distance measuring equipment interference from radio astronomy signals," *Astronomical J.*, vol. 129, no. 6, p. 2933, Jun. 2005.

[17] D. A. Roshi and G. B. NRAO, "RFI mitigation/excision techniques," in *Proc. Spectr. Manage. Radio Astron.*, Jun. 2004, p. 237.

[18] J. M. Ford and K. D. Buch, "RFI mitigation techniques in radio astronomy," in *Proc. IEEE Geosci. Remote Sens. Symp. (IGARSS)*, Jul. 2014, pp. 231–234.

[19] B. D. Van Veen and K. M. Buckley, "Beamforming: A versatile approach to spatial filtering," *IEEE ASSP Mag.*, vol. 5, no. 2, pp. 4–24, Apr. 1988.

[20] S. W. Ellingson, "Beamforming and interference canceling with very large wideband arrays," *IEEE Trans. Antennas Propag.*, vol. 51, no. 6, pp. 1338–1346, Jun. 2003.

[21] J. Raza, A.-J. Boonstra, and A.-J. van der Veen, "Spatial filtering of RF interference in radio astronomy," *IEEE Signal Process. Lett.*, vol. 9, no. 2, pp. 64–67, Feb. 2002.

[22] A. J. Boonstra and S. Van der Tol, "Spatial filtering of interfering signals at the initial low frequency array (LOFAR) phased array test station," *Radio Sci.*, vol. 40, no. 5, pp. 1–16, Oct. 2005.

[23] A. M. Sardarabadi, A.-J. Van Der Veen, and A.-J. Boonstra, "Spatial filtering of RF interference in radio astronomy using a reference antenna array," *IEEE Trans. Signal Process*, vol. 64, no. 2, pp. 432–447, Jan. 2016.

[24] G. C. Bower, "Radio frequency interference mitigation for detection of extended sources with an interferometer," *Radio Sci.*, vol. 40, no. 5, pp. 1–7, Oct. 2005.

[25] M. Kesteven, G. Hobbs, R. Clement, B. Dawson, R. Manchester, and T. Uppal, "Adaptive filters revisited: Radio frequency interference mitigation in pulsar observations," *Radio Sci.*, vol. 40, no. 5, pp. 1–10, Oct. 2005.

[26] J. R. Nagel, K. F. Warnick, B. D. Jeffs, J. R. Fisher, and R. Bradley, "Experimental verification of radio frequency interference mitigation with a focal plane array feed," *Radio Sci.*, vol. 42, no. 6, pp. 1–8, Dec. 2007.

[27] J. Kocz, F. H. Briggs, and J. Reynolds, "Radio frequency interference removal through the application of spatial filtering techniques on the parkes multibeam receiver," *Astronomical J.*, vol. 140, no. 6, p. 2086, Nov. 2010.

[28] B. D. Jeffs, L. Li, and K. F. Warnick, "Auxiliary antenna-assisted interference mitigation for radio astronomy arrays," *IEEE Trans. Signal Process.*, vol. 53, no. 2, pp. 439–451, Feb. 2005.

[29] R. A. Black, B. D. Jeffs, K. F. Warnick, G. Hellbourg, and A. Chippendale, "Multi-tier interference-cancelling array processing for the ASKAP radio telescope," in *Proc. IEEE Signal Process. Signal Process. Educ. Workshop (SP/SPE)*, Aug. 2015, pp. 261–266.

[30] M. E. Abdelgelil and H. Minn, "Non-linear interference cancellation for radio astronomy receivers with strong RFI," in *Proc. IEEE Global Commun. Conf. (GLOBECOM)*, Dec. 2017, pp. 1–6.
[31] M. E. Abdelgelil and H. Minn, "Impact of nonlinear RFI and countermeasure for radio astronomy receivers," *IEEE Access*, vol. 6, pp. 11424–11438, 2018.
[32] H. Minn, Y. R. Ramadan, and Y. Dai, "A new shared spectrum access paradigm between cellular wireless communications and radio astronomy," in *Proc. IEEE Global Commun. Conf. (GLOBECOM)*, Dec. 2016, pp. 1–6.
[33] Y. R. Ramadan, H. Minn, and Y. Dai, "A new paradigm for spectrum sharing between cellular wireless communications and radio astronomy systems," *IEEE Trans. Commun.*, vol. 65, no. 9, pp. 3985–3999, Sep. 2017.
[34] Y. R. Ramadan, Y. Dai, H. Minn, and F. S. Rodrigues, "Spectrum sharing between WiFi and radio astronomy," in *Proc. Radio Freq. Interference (RFI)*, Oct. 2016, pp. 90–95.
[35] D. Han and H. Minn, "Performance analysis of distributed radio telescopes under shared spectrum access paradigm," in *Proc. IEEE Global Commun. Conf. (GLOBECOM)*, Dec. 2017, pp. 1–6.
[36] D. Han and H. Minn, "Performance analysis of distributed auxiliary radio telescopes under shared spectrum access paradigm and cooling power constraint," *IEEE Access*, vol. 5, pp. 21709–21722, 2017.
[37] P. Ayodele and F. Olabisi, "Interference protection of radio astronomy services using cognitive radio spectrum sharing models," in *Proc. Eur. Conf. Netw. Commun. (EuCNC)*, Jun. 2015, pp. 86–90.
[38] Electronic Communications Committee (ECC), "Impact of unwanted emissions of Iridium satellites on radioastronomy operations in the band 1610.6-1613.8 MHz," Tallinn, Estonia, ECC Rep. 171, Oct. 2011.
[39] H. Hirabayashi *et al.*, "The VLBI space observatory programme and the radio-astronomical satellite HALCA," *Publications Astronomical Soc. Jpn.*, vol. 52, no. 6, pp. 955–965, Dec. 2000.
[40] N. S. Kardashev *et al.*, "'RadioAstron'—A telescope with a size of 300 000 km: Main parameters and first observational results," *Astron. Rep.*, vol. 57, no. 3, pp. 153–194, Mar. 2013.
[41] VAO LLC. *U.S. Virtual Astronomical Observatory*. Accessed: Sep. 1, 2018. [Online]. Available: http://www.usvao.org/index.html
[42] *Protection Criteria Used for Radio Astronomical Measurements*, document RA.769-2, ITU-R, 2003.
[43] *Interference calculations Between Non-Geostationary Mobile-Satellite Service or Radionavigation-Satellite Service Systems and Radio Astronomy Telescope Sites*, document M.1583-1, ITU-R, 2007.
[44] OneWeb. (2013). *OneWeb Non-Geostationary Satellite System Attachment A*. [Online]. Available: https://licensing.fcc.gov/myibfs/download.do?attachment_key=1134939
[45] *Satellite Antenna Radiation Pattern for use as a Design Objective in the Fixed-Satellite Service Employing Geostationary Satellites*, document S.672-4, ITU-R, 1997.
[46] D. Wilcoxson, B. Sleight, D. Buchman, and R. VanderMeulen, "Ku-band SATCOM on-the move network," in *Proc. IEEE Mil. Commun. Conf.*, Oct. 2005, pp. 231–237.
[47] J. Zhao, F. Gao, Q. Wu, S. Jin, Y. Wu, and W. Jia, "Beam tracking for UAV mounted SatCom on-the-move with massive antenna array," *IEEE J. Sel. Areas Commun.*, vol. 36, no. 2, pp. 363–375, Feb. 2018.
[48] *Reference FSS Earth-Station Radiation Patterns for Use in Interference Assessment Involving Non-GSO Satellites in Frequency Bands Between, 10.7 GHz and 30 GHz*, document S.1428-1, ITU-R, 2001.
[49] *Manual of Regulations and Procedures for Federal Radio Frequency Management*. Assistant Secretary of Commerce for Communications and Information, Nat. Telecommun. Inf. Admin., Washington, DC, USA, 2014.
[50] FCC. (1996). *Title 47 Part 90.210 : Emission Masks*. [Online]. Available: https://www.gpo.gov/fdsys/pkg/CFR-1996-title47-vol5/pdf/CFR-1996-title47-vol5-sec90-210.pdf
[51] RadioAstron Science and Technical Operations Group. (Mar. 2018). *Radioastron User Handbook*. [Online]. Available: http://www.asc.rssi.ru/radioastron/documents/rauh/en/rauh.pdf
[52] R. Preston *et al.*, "Interferometric observations of an artificial satellite," *Science*, vol. 178, no. 4059, pp. 407–409, Oct. 1972.
[53] J. J. Degnan, "Millimeter accuracy satellite laser ranging: A review," *Contrib. Space Geodesy Geodynamics, Technol.*, vol. 25, pp. 133–162, Jan. 1993.
[54] Netherlands Institute for Radio Astronomy. (2018). *Sensitivity of the LOFAR Array*. [Online]. Available: https://www.astron.nl/radio-observatory/astronomers/lofar-imaging-capabilities-sensitivity/sensitivity-lofar-array/sensiti
[55] J. Wertz and W. J. Larson, *Space Mission Analysis and Design (Space Technology Library)*. El Segundo, CA, USA: Microcosm Press, 1999.

Yucheng Dai (S'18) received the B.S. degree from the Nanjing University of Science and Technology, Nanjing, China, in 2014, and the M.S. degree from Northwestern University, Evanston, IL, USA, in 2015. He is currently pursuing the Ph.D. degree with the Department of Electrical and Computer Engineering, The University of Texas at Dallas, Richardson, TX, USA.

He is currently a Graduate Research Assistant with the Department of Electrical and Computer Engineering, The University of Texas at Dallas. His research interests include wireless communications and signal processing.

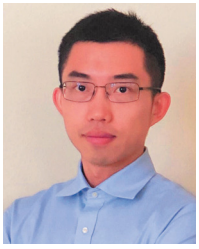

Dong Han (S'17) received the B.E. degree in communication engineering from the University of Electronic Science and Technology of China, Chengdu, China, in 2015, and the M.S. degree in electrical engineering from the National University of Singapore, Singapore, in 2016. He is currently pursuing the Ph.D. degree with the Department of Electrical and Computer Engineering, The University of Texas at Dallas, Richardson, TX, USA. He is a Graduate Research Assistant with the Department of Electrical and Computer Engineering, The University of Texas at Dallas. His research interests include machine-to-machine communications, signal processing, and optimization.

Hlaing Minn (S'99–M'01–SM'07–F'16) received the B.E. degree in electrical electronic engineering from the Yangon Institute of Technology, Yangon, Myanmar, in 1995, the M.E. degree in telecommunications from the Asian Institute of Technology, Thailand, in 1997, and the Ph.D. degree in electrical engineering from the University of Victoria, Victoria, BC, Canada, in 2001.

He was a Post-Doctoral Fellow with the University of Victoria in 2002. He has been with the University of Texas at Dallas, USA, since 2002, where he is currently a Full Professor. His research interests include wireless communications, signal processing, signal design, dynamic spectrum access and sharing, next-generation wireless technologies, and bio-medical signal processing.

Dr. Minn served as a Technical Program Committee Member for over 30 IEEE conferences. He served as a Technical Program Co-Chair for the Wireless Communications Symposium of the IEEE GLOBECOM 2014 and the Wireless Access Track of the IEEE VTC, Fall 2009. He has been serving as an Editor-at-Large, since 2016 and served as an Editor for IEEE TRANSACTIONS ON COMMUNICATIONS from 2005 to 2016. He was also an Editor for *International Journal of Communications and Networks* from 2008 to 2015.